

STA-GANN: A Valid and Generalizable Spatio-Temporal Kriging Approach

Yujie Li

State Key Laboratory of AI Safety,
Institute of Computing Technology,
Chinese Academy of Sciences
University of Chinese Academy of
Sciences
liyujie23s@ict.ac.cn

Tangwen Qian

Zhao Zhang
Yifan Du

State Key Laboratory of AI Safety,
Institute of Computing Technology,
Chinese Academy of Sciences
{qiantangwen,zhangzhao2021}@ict.ac.cn
18810277497duyifan@ict.ac.cn

Zezhi Shao

State Key Laboratory of AI Safety,
Institute of Computing Technology,
Chinese Academy of Sciences
shaozezhi@ict.ac.cn

Shaoming He

School of Aerospace Engineering,
Beijing Institute of Technology
shaoming.he@bit.edu.cn

Chengqing Yu

State Key Laboratory of AI Safety,
Institute of Computing Technology,
Chinese Academy of Sciences
University of Chinese Academy of
Sciences
yuchengqing22b@ict.ac.cn

Fei Wang*

Yongjun Xu

State Key Laboratory of AI Safety,
Institute of Computing Technology,
Chinese Academy of Sciences
University of Chinese Academy of
Sciences
{wangfei,xyj}@ict.ac.cn

Abstract

Spatio-temporal tasks often encounter incomplete data arising from missing or inaccessible sensors, making spatio-temporal kriging crucial for inferring the completely missing temporal information. However, current models struggle with ensuring the validity and generalizability of inferred spatio-temporal patterns, especially in capturing dynamic spatial dependencies and temporal shifts, and optimizing the generalizability of unknown sensors. To overcome these limitations, we propose Spatio-Temporal Aware Graph Adversarial Neural Network (STA-GANN), a novel GNN-based kriging framework that improves spatio-temporal pattern validity and generalization. STA-GANN integrates (i) Decoupled Phase Module that senses and adjusts for timestamp shifts. (ii) Dynamic Data-Driven Metadata Graph Modeling to update spatial relationships using temporal data and metadata; (iii) An adversarial transfer learning strategy to ensure generalizability. Extensive validation across nine datasets from four fields and theoretical evidence both demonstrate the superior performance of STA-GANN.

CCS Concepts

• Information systems → Data mining.

Keywords

spatio-temporal kriging; graph neural networks; transfer learning; graph representation learning

*Corresponding author.



This work is licensed under a Creative Commons Attribution 4.0 International License.
CIKM '25, November 10–14, 2025, Seoul, Republic of Korea
© 2025 Copyright held by the owner/author(s).
ACM ISBN 979-8-4007-2040-6/2025/11
<https://doi.org/10.1145/3746252.3761045>

ACM Reference Format:

Yujie Li, Zezhi Shao, Chengqing Yu, Tangwen Qian, Zhao Zhang, Yifan Du, Shaoming He, Fei Wang, and Yongjun Xu. 2025. STA-GANN: A Valid and Generalizable Spatio-Temporal Kriging Approach. In *Proceedings of the 34th ACM International Conference on Information and Knowledge Management (CIKM '25), November 10–14, 2025, Seoul, Republic of Korea*. ACM, New York, NY, USA, 11 pages. <https://doi.org/10.1145/3746252.3761045>

1 Introduction

Spatio-temporal tasks are crucial in domains such as energy, transportation [36, 37, 55], and meteorology [4], yet sensor unavailability caused by deployment costs, equipment failures often leads to severe data gaps. To mitigate it, spatio-temporal kriging [44] has become a key technique for inferring completely missing time series through temporal and spatial dependencies of available sensors.

The primary challenge of spatio-temporal kriging lies in the absence of time series data for certain unknown sensors or nodes. Unlike conventional time series imputation, which utilizes historical and future data to fill in missing values within the same series, spatio-temporal kriging relies on temporal information from other sensors and their spatial relationships to make inferences. As a result, the model must capture spatio-temporal patterns [22] in both a **valid** and **generalizable** manner. This involves mining meaningful patterns from available data and ensuring these patterns can be transferred to sensors or nodes without prior observations.

Existing methods often struggle to the dual requirements of validity and generalization in spatio-temporal kriging. Traditional approaches, such as Kriging[1] and matrix decomposition[2], typically underperform compared to deep learning models[49] in real-world scenarios. IGNNK[44] is the first to adopt graph neural networks[10, 19] for Kriging, establishing the foundation for subsequent research. SATCN[45], IAGCN[42], and INCREASE[56] all aim to improve performance by extending spatial relationships, but differ in focus: INCREASE leverages scarce metadata including functional areas and points of interest (POIs), while SATCN and IAGCN

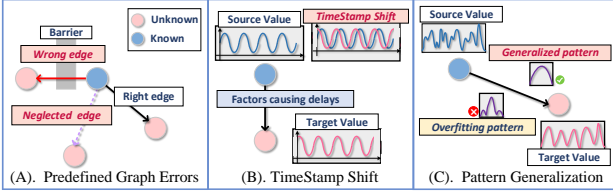


Figure 1: Challenges of Spatio-Temporal Kriging. (A) Predefined graphs may contain unpredictable errors because some edge relations are incorrectly established or ignored. (B) Timestamp shift refers to delays in the transmission of temporal information caused by inevitable factors such as distance and upstream-downstream relationships. (C) The captured overfitted patterns may only be suitable for specific sensors and cannot be generalized.

focus on optimizing the predefined graph [23, 52] or extracting features from it. DualSTN[15] instead targets temporal patterns by disentangling long- and short-term dependencies. However, these methods still face challenges in capturing valid and generalizable spatio-temporal patterns:

- For the validity of spatial patterns, errors in predefined graphs lead to error accumulation during message passing, and current work fails to capture the dynamics of spatial relationships.[20, 47, 54].
- For the validity of temporal patterns [34, 38], timestamp shift poses a unique challenge for kriging, which is distinct from other temporal issues like long-term dependence.
- For the generalization of spatio-temporal patterns to unknown nodes, Label propagation methods for graph-based semi-supervised learning only guarantee convergence [17], but overlooks generalization to unknown sensor patterns.

To address the key challenges of spatio-temporal kriging in terms of validity and generalization, we decompose them into three fundamental challenges and propose corresponding solutions and innovations, as illustrated in Figure 1 :

1. How to ensure the spatial relationship is appropriate?

Spatial relationships are crucial for spatio-temporal kriging. Predefined graphs [23, 52], as shown in Figure 1(A), misrepresent sensor spatial patterns and lack adaptability to environmental changes. This diminishes sensor interactions and causes error accumulation in graph learning, ultimately degrading kriging performance.

OUR APPROACH: We propose **Dynamic Data-Driven Metadata Graph Modeling (D3MGM)** for kriging to capture dynamic spatial dependencies among sensors. This framework leverages temporal data and metadata [21, 27], enabling the model to utilize universal information such as coordinates and timestamps for constructing accurate spatial relationships.

2. How to learn effective temporal patterns?

Timestamp shift in Figure 1(B) [21, 31] refers to the signal transmission delay between sensors. This results in the same information being described at different timestamps across sensors, leading to misalignment with target values and degraded metrics. Moreover, this is a unique problem for spatio-temporal kriging, as forecasting relies on historical data and imputation uses contextual information.

OUR APPROACH: We introduce **Decoupled Phase Module (DPM)** to sense and compensate for timestamp shifts. By adjusting

the phase of unknown sensors in the frequency domain [51, 60] using decoupled series [43], we leverage the Fourier Transform's time-shift property [50] to align timestamps when specific time series information emerges.

3. How to ensure that learned spatio-temporal patterns are generalized? During training, unknown sensors are absent, and missing nodes are simulated by randomly masking known sensors. This raises a critical question: how to ensure the model's generalization to truly unknown sensors and new spatial relationships?

OUR APPROACH: Despite the importance of inductive GNNs for spatio-temporal kriging, it is still difficult to ensure the generalization of spatio-temporal patterns during label propagation. [17]. To address this, we apply adversarial transfer learning[8] to enhance the generalizability[7, 30]. We treat known nodes as the source domain and unknown nodes as the target domain, and introduce discriminators which motivates the model to distinguish between known and unknown sensors. If the model successfully distinguishes them, it suggests a parameter state lacking generalizability. Conversely, maintaining strong kriging performance in this scenario indicates robust generalization.

Overall, we propose **Spatio-Temporal Aware Graph Adversarial Neural Network (STA-GANN)** to address those problems. STA-GANN is a spatio-temporal kriging framework that: (1) constructs dynamic graphs to capture dynamic spatial relationships, (2) detects and compensates for timestamp shifts via a decoupled phase module, and (3) employs adversarial transfer learning to enhance generalization. In the following sections, we detail our approach and demonstrate its effectiveness through theoretical analysis and extensive experiments on multiple real-world datasets. Our contributions are as follows:

- We identify and address the dual challenges of validity and generalization in spatio-temporal kriging, proposing the STA-GANN framework.
- We introduce Dynamic Data-Driven Metadata Graph Modeling and Decoupled Phase Module to perceive valid spatio-temporal patterns.
- We pioneer the focus on generalizability in spatio-temporal kriging, leveraging adversarial transfer learning to ensure the performances.
- We conduct extensive experiments on multiple real-world datasets and perform theoretical proofs to demonstrate the effectiveness of our motivations and methods.

2 Related Work

2.1 Graph Neural Network

Graph Neural Networks[13, 40] are deep learning methods for non-Euclidean graphs. Both GCN[19] and GIN[48] update node representations by aggregating information from neighbors[10], with GIN further controlling historical data and performing nonlinear structural aggregation. Semi-supervised strategies [19], such as randomly masking labeled nodes for reconstruction, are widely adopted in spatio-temporal kriging to enhance performance.

2.2 Spatio-Temporal Forecasting

Spatio-Temporal forecasting[41, 54, 59] is a critical task in multi-variate time series analysis, aiming to predict future time series by

leveraging historical data and spatial relationships. Traffic prediction [23, 37], a prominent subfield, focuses more on spatial dependencies and short-term forecasting. DCRNN[23] utilizes predefined graphs[57], whereas GWNET[47] adaptively learns spatial relationships via learnable node embeddings. Recent works further explore dynamic graph learning [14, 20, 26], which essentially extends GWNET by incorporating dynamic metadata (e.g., timestamps) to infer spatial dependencies. However, in spatio-temporal kriging, **assigning learnable parameters to each node [35, 47] is infeasible due to scalability constraints**. Thus, effectively modeling dynamic spatial dependencies remains a key challenge in our work.

2.3 Spatio-Temporal Imputation & Kriging

Spatio-temporal imputation[53] aims to fill missing values within known nodes, with the primary challenge being the randomness of missing values. However, due to scalability limitations, only a few works such as GRIN[5] are adaptable to kriging after modifications. IGNNK[44] is the first deep kriging model, through GCN and residual network to achieve a good performance of spatio-temporal kriging. SATCN [45] enhances spatial information by exploring predefined graph variants, and DualSTN[15] concerns the analysis of long-term and short-term temporal patterns. Additionally, INCREASE[56] leverages metadata such as POIs and functional areas to construct diverse predefined graphs and prioritizes nearest-neighbor sensors during aggregation. IAGCN [42] expands spatial relations by re-learning from known adjacency matrices.

2.4 Transfer Learning

Transfer learning[9, 29, 61] aims to transfer knowledge from a source domain to a target domain, typically across distinct data distributions. In spatio-temporal kriging, this aligns with transferring patterns from known sensors to unknown sensors. Adversarial transfer learning[32, 39], exemplified by Domain-Adversarial Neural Networks (DANN)[8], employs adversarial training to learn domain-invariant feature representations. This framework typically involves a feature extractor and a domain discriminator: the extractor aims to confuse the discriminator [11], minimizing domain discrepancy to achieve generalization by preventing the discriminator from distinguishing features of the source and target domains.

3 Proposed Method

In this section, we provide an overview of STA-GANN in the order of data flow, and focus on the solutions to three challenges of spatio-temporal kriging presented in Section 1 , including decoupled phase module (DPM) , dynamic data-driven metadata graph modeling (D3MGM) , and adversarial transfer learning strategies.

Problem Definition Let $G_K = \{V_K, E_K, A_K, M_K, X_K\}$ denote the graph of N_K known sensors, where A_K encodes spatial relationships, M_K contains metadata such as coordinates and timestamps, and $X_K = \{X_i\}_{i=1}^{N_K}$ with $X_i = \{x_{i,t}\}_{t=1}^T$ is T -length time series.

Spatio-temporal kriging model \mathcal{F} first learns to reconstruct $\tilde{X}_K = \mathcal{F}(X_K, G_K)$ during training. For unseen sensors $G_U = \{V_U, E_U, A_U, M_U\}$ (Completely missing X_U), it infers $X_U = \mathcal{F}(X_K, G_K + G_U)$ by leveraging learned spatio-temporal dependencies during validation and testing.

3.1 Overview

As depicted in Figure 2, STA-GANN receives:

- Time series $X \in R^{N \times L}$, where unknown sensors initialized as $X_U = 0$,
- Adjacency matrix $A \in R^{N \times N}$ encoding spatial relationships,
- Metadata M ,

We distinguish the data flows with different colors and emphasize that the number of sensors N is arbitrary.

In the encoder, time series first passes through Masked GNN to obtain temporal information, then enters the Decoupled Phase MModule (DPM) to learn timestamp shifts between sensors. We adopt the graph isomorphism network (GIN) as the backbone, The masked GNN resembles GCN but removes GIN’s historical message filtering parameters since unknown sensors lack historical data. The hidden layer dimension of MLPs is denoted as H , the superscript k indicates the k -th MLP layer, and s is a learnable parameter in GIN that controls the strength of history information. The operations of Masked GNN and GIN are defined as follows:

$$X_i^{(k)} = MLP^{(k)} \left(\sum_{j \in V} e_{i,j} \cdot X_j^{(k-1)} \right) = MLP^{(k)}(AX^{(k-1)}) \quad (1)$$

$$\begin{aligned} X_i^{(k)} &= MLP^{(k)} \left((1 + \epsilon^{(k-1)}) \cdot X_i^{(k-1)} + \sum_{j \in V} e_{i,j} \cdot X_j^{(k-1)} \right) \\ &= MLP^{(k)} \left((1 + \epsilon^{(k-1)}) \cdot X_i^{(k-1)} + AX^{(k-1)} \right) \end{aligned} \quad (2)$$

In Masked GNN, predefined graphs are the only source of spatial dependencies. In contrast, the Decoupled Phase Module (DPM) utilizes adjacency matrices generated by Dynamic Data-Driven Metadata Graph Modeling (D3MGM), which derives spatial relationships from temporal information.

For DPM, we highlight its role in sensing and compensating for timestamp shifts during message passing by leveraging frequency-domain information and sensor spatial relationships.

In the decoder, the encoder’s output serves as the initial layer input, with subsequent layers connected sequentially. In Figure 2, the decoder employs a dual-data flow structure, differing in whether the graph network prioritizes sensor self-information. We utilize Masked GNN and GIN, respectively, allowing the convergence layer to adaptively filter dataset-specific information and mitigate error accumulation, a common issue in graph networks. Furthermore, we apply Revin[18] to normalize[28] inputs and inverse-normalize outputs at each layer, reducing the impact of distributional drift.

Furthermore, all GNN outputs preserve the original input dimensions, despite their hidden layer dimension H of the MLPs. Additionally, each $N \times L$ -dimensional vector restores the original information of known sensors during layer-wise propagation and is residually connected to the convergence layer. The convergence layer consists of multiple convolutional layers and performs channel-wise weighting to produce the final output.

In the discriminator, it takes the encoder’s output as input. The discriminator is a simple MLP designed to classify whether the tensors come from known or unknown sensors. Given the limited number of time series, we construct a sliding window of length l , smaller than the time series length, to slice the time series into shorter patches. These patches are then fed into the discriminator for binary classification.

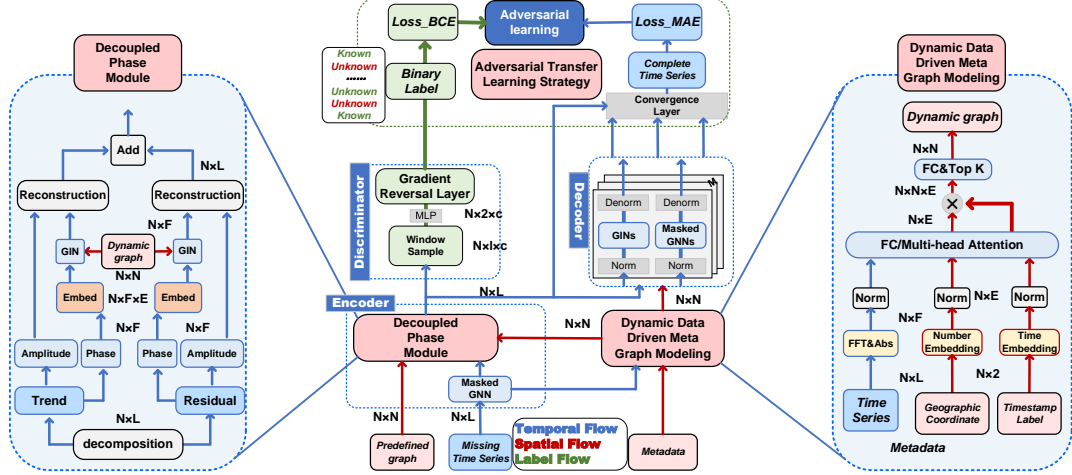


Figure 2: Architecture of STA-GANN

3.2 Dynamic Data-Driven Metadata Graph Modeling

To address the unreliability of predefined graphs, we propose Dynamic Data-Driven Metadata Graph Modeling (D3MGM) to capture dynamic spatial relationships in spatio-temporal kriging. Unlike approaches that assign learnable node parameters in forecasting, D3MGM derives spatial relations directly from temporal data, enriched by metadata including timestamps $Label_{time}$ and coordinates $Label_{coor}$ due to the node variability constraints of kriging.

For timestamps, we follow standard practice in short-term forecasting and construct an index-based lookup table Emb_{time} based on time-of-day and day-of-week, for example, to achieve effective representation of time metadata.

For coordinates, prior methods often depend on dataset-specific preprocessing (e.g., POIs or grid indexing [24, 58]). Instead, we directly embed numerical coordinates by initializing a shared number embedding $Emb_{number} \in R^{N \times E}$ from 0 to 9. Each coordinate is tokenized into digits, and their embeddings are concatenated to form $Emb_{coor} \in R^{N \times E}$, which aligns with the tokenization strategy of large language models like LLaMa for numerical data processing.

Temporal signals are further transformed into the frequency domain $FFT(X) \in R^{N \times F}$ following DFDGCN [21]. Sensor embeddings are then generated via either an attention-based or linear approach, depending on the availability of coordinate information:

$$DE = MHA((Emb_{time} || Emb_{coor}), FFT(X), FFT(X)) \quad (3)$$

$$DE = \text{Linear}(\text{Concat}(Emb_{time}, FFT(X))) \quad (4)$$

To construct the graph structure, we employ the embedding $DE \in R^{N \times E}$ to learn the graph structure. Instead of assigning learnable parameters to DE and its transpose to capture directionality, we introduce a learnable parameter $W_e \in R^E$ to model edge information along dimension E . Finally, the adjacency matrix A_{gm} is generated by selecting the $TopK$ neighbors [46] for each sensor:

$$A_{gm} = TopK(W_e(DE \otimes DE^T)) \quad (5)$$

3.3 Decoupled Phase Module

Decoupled Phase Module (DPM) is employed to sense and complement the timestamp shifts between sensors. The general idea is to decouple the trend and residual components of the time series, allowing the model to learn phase shifts under different components.

Time series decoupling. Time series generally comprise periodic and trend components [16, 25, 60]. Decoupling these components mitigates feature entanglement and facilitates effective temporal modeling. We adopt a standard decomposition method, using average pooling convolutions to extract the trend X^t and residual (periodic) term X^r :

$$X^t = \text{Average}(\text{Pooling}(X)) \quad (6)$$

$$X^r = X - X^t \quad (7)$$

Furthermore, we employ the Fourier Transform to convert time-domain information into the frequency domain, emphasizing amplitude and phase information that are essential for sequence reconstruction. Since timestamp shifts strongly correlate with phase variations, we primarily focus on modeling phase shifts.

The rationale for learning shifts in the frequency rather than time domain lies in its efficiency and reduced risk of overfitting. In this domain, we only model how one phase shifts relative to another based on spatial relationships and their corresponding embeddings. This approach prevents deep learning models from struggling to isolate timestamp shifts and learning irrelevant temporal semantics, which could otherwise potentially lead to overfitting and negatively impact the model's generalization capability and performance.

Phase Embedding: As shown in Figure 3, since the phase range is circular, shifting the phase of the frequency components within this range causes the corresponding time-domain sinusoid to be shifted in the time-stamped dimension. We discretize the range $[-\pi, \pi]$ into M segments, each with a separate embedding, so any phase ϕ_i is represented by an embedding vector $\phi_{i,m}$.

D3MGM constructs the graph A_ϕ during this learning process, enabling specialized GIN to learn the phase shifts effectively. Through GIN, interactions between phase embeddings of each frequency domain component within sequences are facilitated. Ultimately, a fully

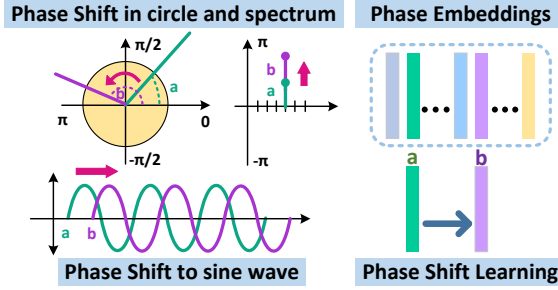


Figure 3: Phase Shift Learning

connected layer transforms high-dimensional phase embeddings into a single one-dimensional phase at the final K -th layer output. Notably, the phase embedding $\vec{\phi}_{i,m}$ remains unlearnable (see Equation 9), while other parameters are trainable. Since it only represents natural information from $-\pi$ to π , random initialization is sufficient to maintain the distinguishability between phase vectors:

$$\vec{\phi}_m = \text{Embedding}(\phi_i) \quad (8)$$

$$\vec{\phi}_{i,m}^k = \text{MLP}((1 + \epsilon^{(k-1)}) \cdot \vec{\phi}_{i,m}^{(k-1)} + A_{\text{phase}} \vec{\Phi}^{(k-1)}) \quad (9)$$

$$\vec{\phi}_i^K = \tanh(\text{FC}(\vec{\phi}_{i,m}^K)) \cdot \pi \quad (10)$$

Upon securing the new phases, we utilize them to reconstruct the time series by performing an inverse Fourier Transform with amplitudes. The trend and residual terms are each subjected to this process independently. Once reconstructed, the time series will be aggregated as the output of DPM and subsequently fed into both the decoder and discriminator components of the system.

Theoretical explanation: The time-shift property of Fourier Transform [6] establishes that temporal translation corresponds to phase rotation in the frequency domain. Let $f(t)$ be a signal with Fourier Transform $F(\omega)$. For any time shift t_0 , the shifted signal $f(t \pm t_0)$ satisfies:

$$\mathcal{F}[f(t \pm t_0)] = e^{\pm j\omega t_0} F(\omega) \quad (11)$$

Generalizing for left/right shifts ($\pm t_0$) and substituting $\phi = \omega t_0$:

$$\mathcal{F}[f(t - t_0)] = e^{-j\phi} F(\omega) \quad (12)$$

$$\mathcal{F}[f(t + t_0)] = e^{j\phi} F(\omega) \quad (13)$$

Applying Euler's formula $e^{\pm j\phi} = \cos \phi \pm j \sin \phi$ and Neglecting imaginary components:

$$\mathcal{F}[f(t \pm t_0)] = [\cos \phi \pm j \sin \phi] F(\omega) \approx \cos \phi \cdot F(\omega) \quad (14)$$

The DPM utilizes a simple transformation of time shift into the frequency domain to learn the phase changes $\phi \in (-\pi, \pi]$ in graphs.

3.4 Adversarial Transfer Learning Strategy

As previously detailed, we apply a sliding window to segment the temporal data $X_{\text{encoder}} \in R^{N \times L}$ from the encoder into shorter patches $X_{\text{patch}} \in R^{N \times l \times c}$, where L refers to the window length of each input and l is a smaller patch length. Subsequently, an MLP-based discriminator is utilized to generate a binary classification label $\text{Label}_D \in R^{N \times 2 \times c}$, as formulated below:

$$\text{Label}_D = \text{MLP}(\text{Window}(X_{\text{encoder}})) \quad (15)$$

The purpose of Label_D is to identify whether the temporal data originates from a known or unknown node. Following the application of the Gradient Reversal Layer (GRL), the discriminator's loss function decreases while the encoder optimizes in an opposing direction. In this adversarial training framework, the discriminator seeks to distinguish between known and unknown nodes, whereas the encoder aims to obscure these distinctions.

In our model, both the discriminator's binary cross-entropy loss Loss_D and Kriging's mean absolute error (MAE) loss $\text{Loss}_{\text{main}}$ are jointly optimized during the initial epochs, where $\text{Loss}_{\text{main}}$ is computed only on missing nodes to ensure the model focuses on reconstructing unavailable sensor data. Due to the instability of adversarial training, we inject a small fraction of noise into the real labels $\text{Label}_{\text{real}}$ for discriminative loss while ensuring that the main loss remains the dominant gradient signal throughout training. The formulation of the loss functions for the initial training stage is as follows:

$$\begin{aligned} \text{Loss} &= \text{Loss}_D + \text{Loss}_{\text{main}} \\ &= \text{BCE}(\text{Label}_D, \text{Label}_{\text{real}}) + \text{Loss}_{\text{main}} \end{aligned} \quad (16)$$

After this stage, the discriminator is frozen.

Theoretical explanation: The theory of our approach [3] is from the classical Generalization Error Bound in the target domain based on \mathcal{H} -divergence for transfer learning. For hypothesis class \mathcal{H} with VC-dim d , with probability $1 - \delta$, $\forall h \in \mathcal{H}$:

$$R_{\mathcal{D}_t}(h) \leq R_s(h) + \hat{d}_{\mathcal{H}}(\mathcal{D}_s, \mathcal{D}_t) + \lambda^* + \sqrt{\frac{4}{n} (d \log \frac{2en}{d} + \log \frac{4}{\delta})} \quad (17)$$

The bound contains four components: (1) empirical source error $R_s(h)$, (2) domain discrepancy $\hat{d}_{\mathcal{H}}$, (3) irreducible term λ^* , and (4) complexity term. As λ^* is intractable with unlabeled target domains, we focus on minimizing $R_s(h)$ ($\text{Loss}_{\text{main}}$) and $\hat{d}_{\mathcal{H}}$ (Loss_D).

Given the known sensor domain \mathcal{D}_s and unknown sensor domain \mathcal{D}_t , X is time series defined over them and a hypothesis class \mathcal{H} . Then the \mathcal{H} -divergence between the two domains $\mathcal{D}_s, \mathcal{D}_t$ is defined as:

$$\hat{d}_{\mathcal{H}}(\mathcal{D}_s, \mathcal{D}_t) = 2 \sup_{\eta \in \mathcal{H}} \left| \mathbb{P}_{\mathbf{x} \in \mathcal{D}_s} [\eta(\mathbf{x}) = 1] - \mathbb{P}_{\mathbf{x} \in \mathcal{D}_t} [\eta(\mathbf{x}) = 1] \right| \quad (18)$$

$$\begin{aligned} \hat{d}_{\mathcal{H}}(\mathcal{D}_s, \mathcal{D}_t) &= 2 \left\{ 1 - \min_{\eta \in \mathcal{H}} \left[\frac{1}{n_1} \sum_{i=1}^{n_1} I[\eta(\mathbf{x}_i) = 0] \right. \right. \\ &\quad \left. \left. + \frac{1}{n_2} \sum_{i=1}^{n_2} I[\eta(\mathbf{x}_i) = 1] \right] \right\} \end{aligned} \quad (19)$$

Optimizing $\hat{d}_{\mathcal{H}}$ turns out to minimize the maximization of the discriminative loss, which we achieve through adversarial learning:

- **Max Step:** Randomly mask known sensors and mislabel them as "unknown" to confuse domains.
- **Min Step:** Optimize BCE loss (Eq.12) to align distributions.

This minmax strategy bridges \mathcal{H} -divergence theory with kriging generalization, analogous to DANN's adversarial mechanism [8].

Table 1: Results of models on nine real datasets. The best results are in bold, and the second best results are underlined.

Datasets	Metrics	STA-GANN	GRIN	INCREASE	DualSTN	IAGCN	IGNNK	SATCN	GCN	GIN	Okriging
METR-LA	MAE	4.887	5.209	5.121	5.9165	6.2377	5.770	5.428	7.68	6.253	8.393
	RMSE	8.012	<u>8.543</u>	8.640	10.228	10.095	9.436	8.792	10.355	9.529	10.959
	R^2	0.861	0.842	0.795	0.774	0.780	0.808	0.636	0.768	0.804	0.741
PEMS-BAY	MAE	3.673	3.708	3.739	3.921	4.399	4.128	4.337	3.993	4.307	4.116
	RMSE	6.495	<u>6.716</u>	6.793	7.152	7.804	7.424	7.968	7.061	8.181	7.247
	R^2	0.593	0.566	0.558	0.507	0.413	0.384	0.389	0.520	0.357	0.494
PEMS03	MAE	64.064	70.044	75.155	75.151	83.161	77.210	73.703	87.816	82.676	77.760
	RMSE	99.443	<u>105.447</u>	116.561	110.662	123.881	115.961	105.722	118.303	117.370	108.324
	R^2	0.576	0.548	0.379	0.440	0.298	0.385	0.489	0.360	0.370	0.464
PEMS04	MAE	59.011	61.256	65.264	61.695	64.848	65.295	76.038	84.149	69.701	69.713
	RMSE	81.992	<u>84.566</u>	91.229	85.329	86.703	90.316	98.956	111.805	89.864	95.659
	R^2	0.674	0.655	0.587	0.639	0.627	0.596	0.515	0.381	0.599	0.546
PEMS07	MAE	69.302	70.779	74.002	80.246	74.639	<u>69.604</u>	88.491	100.749	102.185	83.767
	RMSE	100.190	104.515	107.955	116.376	107.282	<u>102.338</u>	127.582	132.147	134.694	118.140
	R^2	0.71	0.685	0.664	0.610	0.668	0.698	0.531	0.490	0.478	0.598
PEMS08	MAE	86.329	92.291	94.833	93.867	92.145	97.072	93.241	94.014	95.639	91.177
	RMSE	117.203	123.778	124.515	123.573	123.564	135.645	122.677	122.789	125.459	<u>122.092</u>
	R^2	0.417	0.351	0.343	0.352	0.353	0.220	0.362	0.361	0.333	0.358
NREL	MAE	3.965	4.212	4.638	4.415	4.614	4.509	4.417	5.927	4.989	6.508
	RMSE	6.851	7.153	7.444	<u>7.144</u>	7.219	7.267	7.106	8.859	7.694	9.471
	R^2	0.430	0.394	0.327	0.380	0.367	0.359	0.387	0.047	0.281	-0.089
USHCN	MAE	2.190	2.832	2.248	3.912	3.769	2.793	2.767	3.136	3.746	3.158
	RMSE	3.551	4.384	<u>3.771</u>	5.909	5.723	4.312	4.260	4.708	5.663	4.708
	R^2	0.711	0.559	0.674	0.200	0.250	0.572	0.564	0.492	0.265	0.492
AQI	MAE	15.361	16.727	16.626	20.213	27.812	18.162	16.845	23.660	26.478	23.201
	RMSE	27.935	29.944	<u>29.695</u>	34.249	42.544	32.381	30.720	37.498	40.919	36.822
	R^2	0.588	0.528	<u>0.539</u>	0.382	0.046	0.448	0.503	0.260	0.119	0.286

Table 2: Summary of Datasets

Domain	Datasets	Sensors	TimeSteps	Timestamp
Traffic Speed	METR-LA[23]	207	34,272	Mar 2012 - Jun 2012
	PEMS-BAY[23]	325	52,116	Jan 2017 - Jun 2017
Traffic Flow	PEMS03	358	26,208	Sep 2018 - Nov 2018
	PEMS04 [12]	307	16,992	Jan 2018 - Feb 2018
	PEMS07	883	28,224	May 2017 - Aug 2017
	PEMS08	170	17,856	Jul 2016 - Aug 2016
Energy	NREL[44]	137	105,120	2006
Weather	USHCN[44]	1,218	1,440	1899 - 2019
Environment	AQI[5]	437	59,710	Jan 2015 to Dec 2022

4 Experiments

4.1 Datasets

Datasets: We evaluate STA-GANN on nine real-world datasets across four domains in Table 2. Sensors are split into training (Known), validation (Unknown), and testing (Unknown) sets in a 7:1:2 ratio, while time steps are partitioned 7:3 for trained and untrained intervals. Temporal data and metadata of unknown sensors are unavailable during training.

Baselines and Metrics: STA-GANN is compared against: (1) pure GNNs such as GCN [19] and GIN [48]; (2) spatio-temporal kriging models like IGN NK [44], SATCN [45], INCREASE [56], DualSTN[15] and IAGCN[42] ; (3) GRIN[5], a SOTA imputation model adapted for kriging; (4) Parameter-free Okriging aggregating 1st-order neighbor messages. Performance is measured by Mean Absolute Error (MAE), Root Mean Square Error (RMSE), and the coefficient of determination R^2 .

Hyperparameters: Table 3 summarizes the main hyperparameters, with others following baseline defaults. Series-level embedding such as STA-GANN are used with temporal dimension set to 100,

Table 3: Summary of Parameters

Parameter Name	Description
Length of Time Series L	24
Number of Training Rounds	50
Batch Size	64
Optimizer	Adam
Loss	MAE (+ our BCE)
Metadata Embedding Dimension F	20
Adversarial Strategy Rounds	5
Label Embedding Dimension E	12
Dropout Rate	0.3
Temporal Embedding Dimension H	100 (IGN NK, GNNs, DualSTN, IAGCN, STA-GANN) 16 (others)
Learning Rate	0.003 (Most) 0.01 (GRIN, INCREASE)
Predefined graph	Original (Most) Random-Walk (SATCN)
TopK(ours)	50 (PEMS0X) 5 (others)

while timestep-based embeddings use a dimension of 16; SATCN exclusively uses a predefined random walk graph, while STA-GANN and others typically rely on the native dataset graphs.

Our Kriging process is based on the spatio-temporal benchmark BasicTS [33], our code is publicly available to facilitate reproducibility and further research: <https://github.com/blisky-li/STAGANN>.

4.2 Main Results

As shown in Table 1, STA-GANN achieves state-of-the-art performance across nine real-world datasets, with consistent improvements of over 5% compared to existing baselines. Particularly, it not

Table 4: Ablation study of STA-GANN, *italics* indicate variants that have lost the corresponding module. The best results are in bold, and the second best results. are underlined.

Datasets	Metrics	STA-GANN	STA-GANN-S	-S-location	-S-timestamp	STA-GANN-T	-T-phagegraph	-T-decouple	STA-GANN-A	-A10	-A50	STA-GANN- <i>Revin</i>
METR-LA	MAE	4.887	5.122	4.948	5.095	5.068	5.069	4.973	5.235	4.962	4.928	4.914
	RMSE	<u>8.012</u>	8.306	8.003	8.048	8.195	8.170	8.112	8.353	8.138	8.089	<u>8.032</u>
PEMS08	MAE	86.329	91.122	-	89.706	91.692	90.362	87.850	89.326	87.623	87.723	87.842
	RMSE	117.203	120.899	-	119.568	121.116	120.025	118.239	120.261	<u>117.624</u>	117.895	117.982
NREL	MAE	3.965	4.191	3.976	4.125	4.065	4.145	4.009	4.062	3.927	4.020	3.972
	RMSE	<u>6.851</u>	6.924	6.848	6.916	6.889	6.968	6.865	6.902	6.780	6.863	6.823
USHCN	MAE	2.190	2.267	2.217	2.241	2.215	2.215	2.204	2.230	2.205	2.183	2.197
	RMSE	3.551	3.810	3.750	3.706	3.638	3.784	3.613	3.696	3.633	<u>3.587</u>	3.623

only surpasses spatio-temporal kriging methods like INCREASE, DualSTN and IAGCN but also achieves nearly a 10% improvement on datasets such as PEMS0X, NREL, and AQI. This enhanced performance is attributed to the model’s ability to validly capture spatio-temporal patterns between sensors and generalize these patterns to unknown sensors. The unmodified GIN and GCN exhibit performance comparable to OKriging in the Kriging problem. Regarding graph learning methods, both SATCN and IAGCN operate on predefined graphs, which amplifies error accumulation. While DualSTN, INCREASE, and GRIN demonstrate improvements in temporal learning, their performance remains constrained by unreliable pre-defined graph. Furthermore, lacking strategies to enhance generalization capability, these methods may achieve good performance on certain datasets but suffer from significant performance degradation in others due to overfitting issues.

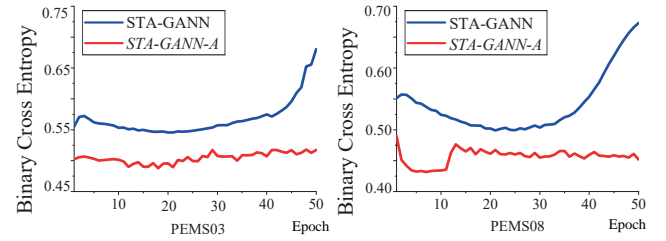
4.3 Ablation Study

To assess the contributions of STA-GANN’s components, we perform ablation studies by progressively removing key modules and strategies. Notation “-S/-T/-A” indicates the removal of D3MGM, DPM, and adversarial transfer learning strategies. Furthermore, -S-*location/-timestamp* remove of location or timestamp information in Equation 3; -T-*phagegraph/-decouple* replaces dynamic graphs in Equation 9 with predefined graphs, and removes time-series decoupling from Equations 6 and 7; -A10/A50 freezes the discriminator after 10 rounds or applies no freezing.

We evaluate on four representative datasets (METR-LA, PEMS08, NREL, and USHCN) covering diverse scenarios. Additionally, we remove Revin in the decoder, which shows negligible impact.

As shown in Table 4, STA-GANN consistently outperforms its ablation variants. Notably, Removing D3MGM in STA-GANN-S causes a performance drop exceeding 4%, highlighting its critical role in enhancing model effectiveness. Both location and timestamp information are essential for accurate graph modeling, with timestamps being particularly influential. These results confirm that predefined graphs often contain inherent biases, while dynamic spatial dependencies captured by D3MGM effectively mitigate such limitations.

From the results in Table 4, both DPM and adversarial transfer learning demonstrate benefits, though they show sensitivity to specific data patterns. DPM requires stable periodicity and timestamp shifts for improvements, and the “-phagegraph” also confirms the importance of spatial relationships, and time-series decoupling largely has the effect of maintaining model stability.

**Figure 4: Confusion between known and unknown sensors on PEMS03 and PEMS08**

The adversarial transfer learning strategy shows limited effectiveness when patterns are too similar or too different. While freezing the discriminator after round 5 provides acceptable results, other rounds may yield better performance, though optimizing this parameter remains challenging due to adversarial methods’ inherent limitations. Fortunately, this strategy in METR-LA still provides the most significant improvement compared to D3MGM and DPM.

4.4 Pattern Confusion

We present the first study on the generalizability of spatio-temporal kriging, focusing on pattern confusion through controlled tests.

To address the fundamental challenge of ensuring generalizability between sensors, we employ the adversarial transfer learning strategy, introducing a discriminator with a gradient reversal layer to enforce domain invariance. To evaluate its effect, we test STA-GANN against STA-GANN-A to evaluate generalizability, which includes all components except adversarial training. We incorporate an unlearnable discriminator into STA-GANN-A to detect the classification loss on the PEMS03 and PEMS08 test sets in Figure 4.

The BCE loss of STA-GANN-A remains smooth, with a brief initial drop on PEMS08 due to overly unique patterns learned from known sensors. In contrast, STA-GANN’s loss decreases slowly at first but rises sharply after the discriminator is frozen, implying that the model maintains domain invariance between sensors.

In STA-GANN, the discriminator learns to distinguish the domains of sensors, while the gradient reversal layer reverses the update direction, preventing reliable distinction between known and unknown sensors. It forces the encoder to confuse sensor domains, leading to indistinguishable domains at later stages and the BCE loss increase—evidence of successful generalization.

In summary, an increase in BCE loss on the test set signals that the adversarial strategy has masked sensor-specific features, enabling STA-GANN to generalize from known to unknown sensors, validating both our motivations and the effectiveness of the proposed method.

4.5 Missing Rate Experiment

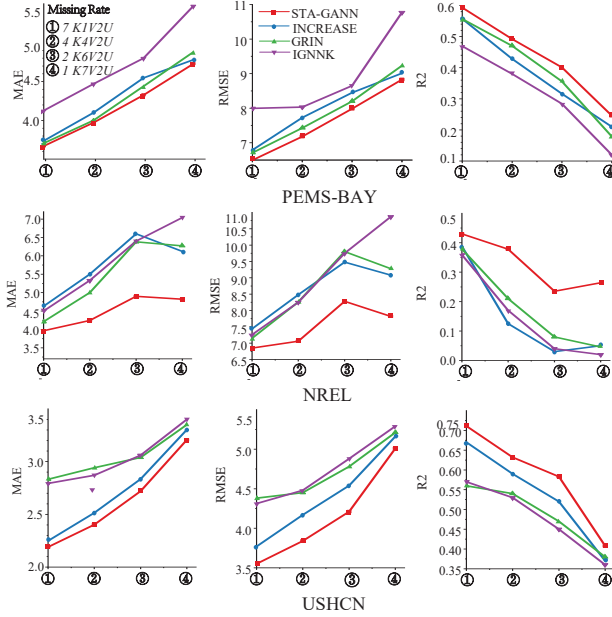


Figure 5: Experimental results for the missing rate

Missing rate of sensors is a critical issue in spatio-temporal kriging, and we conduct experiments to simulate different missing rate scenarios in reality. In our notation, $xKyVzU$ indicates that $10\% \times x$ sensors are known, and $10\% \times z$ sensors are unknown in the test set, the remaining sensors are unknown sensors in the validation set. Our focus lies on analyzing the spatio-temporal patterns derived from the $10\% \times x$ known sensors and evaluating the performance on the $10\% \times z$ sensors. To ensure consistency in our evaluation, we fix $z = 2$ (representing fixed 20% unknown sensors), and varied the number of known sensor across four configurations: $x = 7, 4, 2, 1$. For example, when $x = 1$, the known sensors must extrapolate to twice as many unknown sensors.

We conduct experiments on the PEMS-BAY, NREL, and USHCN datasets and report metrics such as MAE, RMSE, and R2. The performance of the STA-GANN model was compared against three novel models: IGNNK, INCREASE, and GRIN. The results, presented in Figure 5, reveal a consistent trend: the performance of all models deteriorates as the missing rate increases. However, an intriguing observation emerged for the NREL dataset: the performance at $x = 2$ is worse than $x = 1$. This discrepancy could be attributed to the fact that additional known sensors introduced after randomization may not exhibit strong correlations with the unknown sensors, potentially hindering the propagation of temporal information.

Despite this anomaly in the NREL dataset, STA-GANN demonstrate superior robustness across all datasets. Its ability to consistently outperform other models, even as the missing rate increases,

underscores its effectiveness in capturing valid spatio-temporal patterns and generalizing them to unknown sensors. This capability is particularly valuable in scenarios with sparse sensor data, where traditional methods often struggle to maintain accuracy.

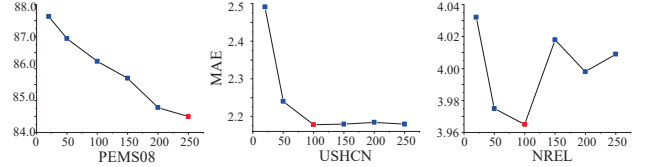


Figure 6: Experimental results for MLP embedding size

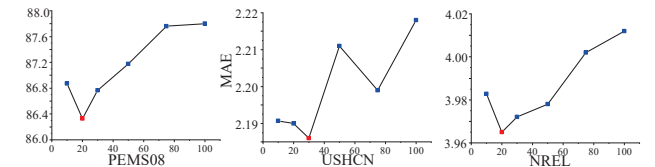


Figure 7: Experimental results for metadata embedding size

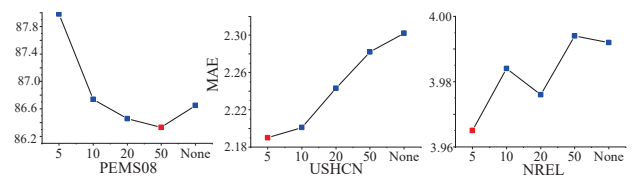


Figure 8: Experimental results for the K in adjacency matrix

4.6 Parameter study

For temporal embeddings, as shown in Figure 6, performance improves with larger dimensions but shows diminishing returns beyond 100, with potential overfitting on the NREL dataset. Metadata embedding dimensionality also requires careful tuning in Figure 7. While larger embeddings may lead to overfitting and degraded performance, a range of 20–30 typically balances model capacity and generalization effectively. Regarding the TopK parameter in the adjacency matrix, sensitivity varies across datasets as demonstrated in Figure 8. PEMS08 and NREL show stable performance across different TopK values, while USHCN demonstrates higher sensitivity, likely due to geographic and climatic differences across regions within the United States.

4.7 Runtime experiment

We record the complete runtime of the training, validation, and testing periods of all the models in the main experiment, runtime in hours is shown in Table 5.

We can find that STA-GANN is in an intermediate runtime performance. GRIN and INCREASE, which have the highest accuracy performance among the extrapolation baselines, are both at very high runtimes, while we achieve the best accuracy and keep the runtimes much lower than them. IGNNK, SATCN, and the two graph networks GCN and GIN are both shorter but have correspondingly much lower accuracies.

Table 5: Runtime of STA-GANN and Baselines on nine real datasets

Runtime(hours)	STA-GANN	GRIN	INCREASE	DualSTN	IAGCN	IGNNK	SATCN	GCN	GIN
METR-LA	0.75	2.22	3.48	0.95	5.2	0.4	0.525	0.15	0.18
PEMS-BAY	1.04	3.66	4.16	1.73	10.37	0.25	0.46	0.21	0.24
PEMS03	0.44	1.89	3.72	1.1	8.2	0.21	0.25	0.18	0.21
PEMS04	0.30	1.30	2.71	0.7	3.7	0.24	0.28	0.17	0.17
PEMS07	1.70	7.03	12.05	3.83	20.35	0.48	0.79	0.36	0.42
PEMS08	0.33	0.92	1.72	0.5	2.62	0.13	0.12	0.10	0.10
NREL	1.67	4.73	8.04	2.12	12.5	0.37	0.59	0.32	0.41
USHCN	0.23	0.51	0.90	0.72	3.2	0.16	0.21	0.08	0.10
AQI	1.38	4.57	7.89	2.47	18.25	0.30	0.37	0.28	0.32

In short, the computational complexity of STA-GANN arises from the GIN network ($O(NH^2)$) and D3MGM ($O(N^2E)$). GIN’s complexity is slightly higher than that of GCN due to the additional MLP layers, while D3MGM’s complexity is comparable to that in typical spatio-temporal forecasting tasks. In comparison, the computational cost of GRIN and INCREASE mainly comes from timestep-based GCN ($O(N^2HL)$), while IAGCN incurs additional overhead due to graph decomposition and learning ($O(N^3E)$).

In summary, STA-GANN not only has the best accuracy for extrapolation, the running time is much lower than the current best Baselines and is not significantly higher than the other models.

4.8 Time Shift visualization

We design the DPM module to learn timestamp shifts. To visualize the effect of this module, we select three sensors in USHCN and show their time series at the input and output of the DPM in Figure 9. We can observe that instead of learning the representation of time series, the DPM tries to change the phase, realizing the problem of translating the series in the timestamp dimension to accommodate the shifts, which are not exactly the same shape since we restrict only the phase of the primary frequency can be modified.

5 Limitation

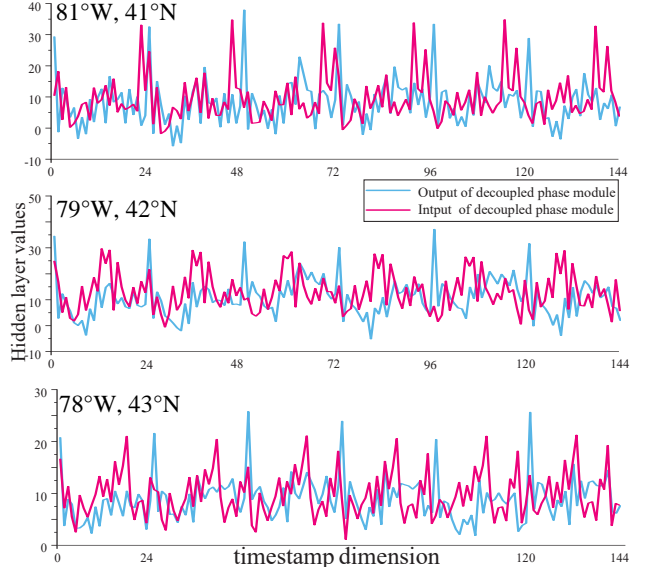
Metadata Dependency: Performance degrades with missing or inaccurate coordinates or timestamp shifts.

Scalability: While node-scalable, the model falters on: (1) coordinate extrapolation in small datasets, (2) fixed-length constraints hindering real-time kriging.

Range Variation: Failure to adapt to unknown sensors’ value ranges causes inference discrepancies (Table 1).

6 Conclusion

In this paper, we address the fundamental challenges of spatio-temporal kriging, particularly focusing on validity and generalization. To overcome these challenges, we present our Spatio-Temporal Aware Graph Adversarial Neural Network (STA-GANN). Our key contributions include threefold: First, we introduce a decoupled phase module to effectively recover timestamp shifts among sensors, ensuring the temporal validity of patterns. Second, we propose a dynamic data-driven metadata graph modeling approach to capture spatial dependencies among sensors, thereby establishing spatial

**Figure 9: Outputs and inputs of Decoupled Phase Module**

pattern validity. Third, for generalizability, we employ an adversarial transfer learning strategy that enables the effective extrapolation of spatio-temporal patterns from known to unknown sensors.

Considering the wide range of real-world applications of spatio-temporal kriging, we hope that our work will inspire further investigation and advancements in this field. In the future, we will continue to focus on spatio-temporal kriging, including improving the scalability of online kriging, more sophisticated nonlinear timestamp drift and magnitude forecasting, and maintaining the Benchmark for spatio-temporal kriging.

7 Acknowledgments

This work is supported by NSFC No.62372430, the Youth Innovation Promotion Association CAS No.2023112, the Postdoctoral Fellowship Program of CPSF under Grant Number GZC20251078, the China Postdoctoral Science Foundation No.2025M77154 and HUA Innovation fundings. We thank all the anonymous reviewers who generously contributed their time and efforts.

GenAI Usage Disclosure

The proposed methodology, experiments, the datasets used and the code in our paper do not use GenAI. We adopt ChatGPT to edit and improve the quality of existing text and strictly prohibit it from searching web content.

References

- [1] Gabriel Appleby, Linfeng Liu, and Li-Ping Liu. 2020. Kriging convolutional networks. In *AAAI*, Vol. 34. 3187–3194.
- [2] Mohammad Taher Bahadori, Qi Rose Yu, and Yan Liu. 2014. Fast multivariate spatio-temporal analysis via low rank tensor learning. *NeurIPS* 27 (2014).
- [3] Shai Ben-David, John Blitzer, Koby Crammer, Alex Kulesza, Fernando Pereira, and Jennifer Wortman Vaughan. 2010. A theory of learning from different domains. *Machine learning* 79 (2010), 151–175.
- [4] Kaifeng Bi, Lingxi Xie, Hengheng Zhang, Xin Chen, Xiaotao Gu, and Qi Tian. 2023. Accurate medium-range global weather forecasting with 3D neural networks. *Nature* 619, 7970 (2023), 533–538.
- [5] Andrea Cini, Ivan Marasca, and Cesare Alippi. 2021. Filling the G_ap_s: Multivariate Time Series Imputation by Graph Neural Networks. In *ICLR*.
- [6] Berken Utku Demirel and Christian Holz. 2025. Shifting the Paradigm: A Diffeomorphism Between Time Series Data Manifolds for Achieving Shift-Invariancy in Deep Learning. *arXiv preprint arXiv:2502.19921* (2025).
- [7] Yuntao Du, Jindong Wang, Wenjie Feng, Sinno Pan, Tao Qin, Renjun Xu, and Chongjun Wang. 2021. Adarmn: Adaptive learning and forecasting of time series. In *CIKM*. 402–411.
- [8] Yaroslav Ganin, Evgeniya Ustinova, Hana Ajakan, Pascal Germain, Hugo Larochelle, François Laviolette, Mario March, and Victor Lempitsky. 2016. Domain-adversarial training of neural networks. *JMLR* 17, 59 (2016), 1–35.
- [9] Muhammad Ghifary, W Bastiaan Kleijn, and Mengjie Zhang. 2014. Domain adaptive neural networks for object recognition. In *PRICAL*. 898–904.
- [10] Justin Gilmer, Samuel S Schoenholz, Patrick F Riley, Oriol Vinyals, and George E Dahl. 2017. Neural message passing for quantum chemistry. In *ICML*. PMLR, 1263–1272.
- [11] Ian Goodfellow, Jean Pouget-Abadie, Mehdi Mirza, Bing Xu, David Warde-Farley, Sherjil Ozair, Aaron Courville, and Yoshua Bengio. 2014. Generative adversarial nets. *NeurIPS* 27 (2014).
- [12] Shengnan Guo, Youfang Lin, Huaiyu Wan, Xiucheng Li, and Gao Cong. 2021. Learning dynamics and heterogeneity of spatial-temporal graph data for traffic forecasting. *TKDE* 34, 11 (2021), 5415–5428.
- [13] Will Hamilton, Zhitao Ying, and Jure Leskovec. 2017. Inductive representation learning on large graphs. *NeurIPS* 30 (2017).
- [14] Liangzhe Han, Bowen Du, Leilei Sun, Yanjie Fu, Yisheng Lv, and Hui Xiong. 2021. Dynamic and multi-faceted spatio-temporal deep learning for traffic speed forecasting. In *KDD*. 547–555.
- [15] Junfeng Hu, Yuxuan Liang, Zhencheng Fan, Li Liu, Yifang Yin, and Roger Zimmermann. 2023. Decoupling long- and short-term patterns in spatiotemporal inference. *IEEE Transactions on Neural Networks and Learning Systems* (2023).
- [16] Norden E Huang, Zheng Shen, Steven R Long, Manli C Wu, Hsing H Shih, Quanran Zheng, Nai-Chyuan Yen, Chi Chao Tung, and Henry H Liu. 1998. The empirical mode decomposition and the Hilbert spectrum for nonlinear and non-stationary time series analysis. *Proceedings of the Royal Society of London. Series A: mathematical, physical and engineering sciences* 454, 1971 (1998), 903–995.
- [17] Ahmet Iscen, Giorgos Tolias, Yannis Avrithis, and Ondrej Chum. 2019. Label propagation for deep semi-supervised learning. In *Proceedings of the IEEE/CVF conference on computer vision and pattern recognition*. 5070–5079.
- [18] Taesung Kim, Jinhee Kim, Yunwon Tae, Cheonbok Park, Jang-Ho Choi, and Jaegul Choo. 2021. Reversible instance normalization for accurate time-series forecasting against distribution shift. In *ICLR*.
- [19] Thomas N Kipf and Max Welling. 2017. Semi-Supervised Classification with Graph Convolutional Networks. In *ICLR*.
- [20] Fuxian Li, Jie Feng, Huan Yan, Guangyin Jin, Fan Yang, Funing Sun, Depeng Jin, and Yong Li. 2023. Dynamic graph convolutional recurrent network for traffic prediction: Benchmark and solution. *TKDD* 17, 1 (2023), 1–21.
- [21] Yujie Li, Zexhi Shao, Yongjun Xu, Qiang Qiu, Zhaogang Cao, and Fei Wang. 2024. Dynamic Frequency Domain Graph Convolutional Network for Traffic Forecasting. In *ICASSP*. IEEE, 5245–5249.
- [22] Yujie Li, Tao Sun, Zexhi Shao, Yiqiang Zhen, Yongjun Xu, and Fei Wang. 2025. Trajectory-User Linking via Multi-Scale Graph Attention Network. *Pattern Recognition* 158 (2025), 110978.
- [23] Yaguang Li, Rose Yu, Cyrus Shahabi, and Yan Liu. 2018. Diffusion Convolutional Recurrent Neural Network: Data-Driven Traffic Forecasting. In *ICLR*.
- [24] Ke Liang, Lingyuan Meng, Hao Li, Meng Liu, Siwei Wang, Sihang Zhou, Xinwang Liu, and Kunlun He. 2024. MGKsite: Multi-Modal Knowledge-Driven Site Selection via Intra and Inter-Modal Graph Fusion. *IEEE Transactions on Multimedia* (2024).
- [25] Ke Liang, Lingyuan Meng, Meng Liu, Yue Liu, Wenxuan Tu, Siwei Wang, Sihang Zhou, and Xinwang Liu. 2023. Learn from relational correlations and periodic events for temporal knowledge graph reasoning. In *Proceedings of the 46th international ACM SIGIR conference on research and development in information retrieval*. 1559–1568.
- [26] Ke Liang, Lingyuan Meng, Meng Liu, Yue Liu, Wenxuan Tu, Siwei Wang, Sihang Zhou, Xinwang Liu, Fuchun Sun, and Kunlun He. 2024. A survey of knowledge graph reasoning on graph types: Static, dynamic, and multi-modal. *IEEE Transactions on Pattern Analysis and Machine Intelligence* (2024).
- [27] Xu Liu, Yutong Xia, Yuxuan Liang, Junfeng Hu, Yiwei Wang, Lei Bai, Chao Huang, Zhengguang Liu, Bryan Hooi, and Roger Zimmermann. 2024. Largest: A benchmark dataset for large-scale traffic forecasting. *NeurIPS* 36 (2024).
- [28] Yong Liu, Haixi Wu, Jianmin Wang, and Mingsheng Long. 2022. Non-stationary transformers: Exploring the stationarity in time series forecasting. *NeurIPS* 35 (2022), 9881–9893.
- [29] Mingsheng Long, Han Zhu, Jianmin Wang, and Michael I Jordan. 2017. Deep transfer learning with joint adaptation networks. In *ICML*. PMLR, 2208–2217.
- [30] Wang Lu, Jindong Wang, Xinwei Sun, Yiqiang Chen, and Xing Xie. 2022. Out-of-distribution Representation Learning for Time Series Classification. In *ICLR*.
- [31] Hao Niu, Guillaume Habault, Roberto Legaspi, Chuizheng Meng, Defu Cao, Shinya Wada, Chihiro Ono, and Yan Liu. 2023. Time-delayed Multivariate Time Series Predictions. In *SDM*. SIAM, 325–333.
- [32] Kuniaki Saito, Kohei Watanabe, Yoshitaka Ushiku, and Tatsuya Harada. 2018. Maximum classifier discrepancy for unsupervised domain adaptation. In *CVPR*. 3723–3732.
- [33] Zexhi Shao, Fei Wang, Yongjun Xu, Wei Wei, Chengqing Yu, Zhao Zhang, Di Yao, Tao Sun, Guangyin Jin, Xin Cao, et al. 2024. Exploring progress in multivariate time series forecasting: Comprehensive benchmarking and heterogeneity analysis. *IEEE Transactions on Knowledge and Data Engineering* 37, 1 (2024), 291–305.
- [34] Zexhi Shao, Fei Wang, Zhao Zhang, Yuchen Fang, Guangyin Jin, and Yongjun Xu. 2023. HUTformer: Hierarchical U-Net Transformer for Long-Term Traffic Forecasting. *arXiv preprint arXiv:2307.14596* (2023).
- [35] Zexhi Shao, Zhao Zhang, Fei Wang, Wei Wei, and Yongjun Xu. 2022. Spatial-temporal identity: A simple yet effective baseline for multivariate time series forecasting. In *CIKM*. 4454–4458.
- [36] Zexhi Shao, Zhao Zhang, Fei Wang, and Yongjun Xu. 2022. Pre-training enhanced spatial-temporal graph neural network for multivariate time series forecasting. In *KDD*. 1567–1577.
- [37] Zexhi Shao, Zhao Zhang, Wei Wei, Fei Wang, Yongjun Xu, Xin Cao, and Christian S Jensen. 2022. Decoupled dynamic spatial-temporal graph neural network for traffic forecasting. *Proceedings of the VLDB Endowment* 15, 11 (2022), 2733–2746.
- [38] Shun-Yao Shih, Fan-Keng Sun, and Hung-yi Lee. 2019. Temporal pattern attention for multivariate time series forecasting. *Machine Learning* 108 (2019), 1421–1441.
- [39] Baochen Sun and Kate Saenko. 2016. Deep coral: Correlation alignment for deep domain adaptation. In *ECCV*. Springer, 443–450.
- [40] Petar Veličković, Guillem Cucurull, Arantxa Casanova, Adriana Romero, Pietro Liò, and Yoshua Bengio. 2018. Graph Attention Networks. In *ICLR*.
- [41] Yuan Wang, Zexhi Shao, Tao Sun, Chengqing Yu, Yongjun Xu, and Fei Wang. 2023. Clustering-property Matters: A Cluster-aware Network for Large Scale Multivariate Time Series Forecasting. In *CIKM*. 4340–4344.
- [42] Tonglong Wei, Youfang Lin, Shengnan Guo, Yan Lin, Yiji Zhao, Xiyuan Jin, Zhihao Wu, and Huaiyu Wan. 2024. Inductive and adaptive graph convolution networks equipped with constraint task for spatial-temporal traffic data kriging. *Knowledge-Based Systems* 284 (2024), 111325.
- [43] Haixu Wu, Jiehui Xu, Jianmin Wang, and Mingsheng Long. 2021. Autoformer: Decomposition transformers with auto-correlation for long-term series forecasting. *NeurIPS* 34 (2021), 22419–22430.
- [44] Yuankai Wu, Dingyi Zhuang, Aurelie Labbe, and Lijun Sun. 2021. Inductive graph neural networks for spatiotemporal kriging. In *AAAI*, Vol. 35. 4478–4485.
- [45] Yuankai Wu, Dingyi Zhuang, Mengying Lei, Aurelie Labbe, and Lijun Sun. 2021. Spatial aggregation and temporal convolution networks for real-time kriging. *arXiv preprint arXiv:2109.12144* (2021).
- [46] Zonghan Wu, Shirui Pan, Guodong Long, Jing Jiang, Xiaojun Chang, and Chengqi Zhang. 2020. Connecting the dots: Multivariate time series forecasting with graph neural networks. In *KDD*. 753–763.
- [47] Zonghan Wu, Shirui Pan, Guodong Long, Jing Jiang, and Chengqi Zhang. 2019. Graph wavenet for deep spatial-temporal graph modeling. In *IJCAI*. 1907–1913.
- [48] Keyulu Xu, Weihua Hu, Jure Leskovec, and Stefanie Jegelka. 2019. How Powerful are Graph Neural Networks? In *ICLR*.
- [49] Yongjun Xu, Xin Liu, Xin Cao, and et al. 2021. Artificial intelligence: A powerful paradigm for scientific research. *The Innovation* 2, 4 (2021).
- [50] Zhangjing Yang, Weiwu Yan, Xiaolin Huang, and Lin Mei. 2020. Adaptive temporal-frequency network for time-series forecasting. *TKDE* 34, 4 (2020), 1576–1587.
- [51] Kun Yi, Qi Zhang, Wei Fan, Shoujin Wang, Pengyang Wang, Hui He, Ning An, Defu Lian, Longbing Cao, and Zhendong Niu. 2024. Frequency-domain MLPs

- are more effective learners in time series forecasting. *NeurIPS* 36 (2024).
- [52] Bing Yu, Haoteng Yin, and Zhanxing Zhu. 2018. Spatio-Temporal Graph Convolutional Networks: A Deep Learning Framework for Traffic Forecasting. In *IJCAI*.
- [53] Chengqing Yu, Fei Wang, Zezhi Shao, Tangwen Qian, Zhao Zhang, Wei Wei, Zhulin An, Qi Wang, and Yongjun Xu. 2025. GinAR+: A Robust End-To-End Framework for Multivariate Time Series Forecasting with Missing Values. *IEEE Transactions on Knowledge and Data Engineering* (2025).
- [54] Chengqing Yu, Fei Wang, Zezhi Shao, Tao Sun, Lin Wu, and Yongjun Xu. 2023. Dsformer: A double sampling transformer for multivariate time series long-term prediction. In *CIKM*. 3062–3072.
- [55] Chuanpan Zheng, Xiaoliang Fan, Cheng Wang, and Jianzhong Qi. 2020. Gman: A graph multi-attention network for traffic prediction. In *AAAI*, Vol. 34. 1234–1241.
- [56] Chuanpan Zheng, Xiaoliang Fan, Cheng Wang, Jianzhong Qi, Chaochao Chen, and Longbiao Chen. 2023. Increase: Inductive graph representation learning for spatio-temporal kriging. In *WWW*. 673–683.
- [57] Chuanpan Zheng, Xiaoliang Fan, Chenglu Wen, Longbiao Chen, Cheng Wang, and Jonathan Li. 2019. DeepSTD: Mining spatio-temporal disturbances of multiple context factors for citywide traffic flow prediction. *TITS* 21, 9 (2019), 3744–3755.
- [58] Chuanpan Zheng, Cheng Wang, Xiaoliang Fan, Jianzhong Qi, and Xu Yan. 2021. STPC-Net: Learn massive geo-sensory data as spatio-temporal point clouds. *TITS* 23, 8 (2021), 11314–11324.
- [59] Haoyi Zhou, Shanghang Zhang, Jieqi Peng, Shuai Zhang, Jianxin Li, Hui Xiong, and Wancai Zhang. 2021. Informer: Beyond efficient transformer for long sequence time-series forecasting. In *AAAI*, Vol. 35. 11106–11115.
- [60] Tian Zhou, Ziqing Ma, Qingsong Wen, Xue Wang, Liang Sun, and Rong Jin. 2022. Fedformer: Frequency enhanced decomposed transformer for long-term series forecasting. In *ICML*. PMLR, 27268–27286.
- [61] Fuzhen Zhuang, Zhiyuan Qi, Keyu Duan, Dongbo Xi, Yongchun Zhu, Hengshu Zhu, Hui Xiong, and Qing He. 2020. A comprehensive survey on transfer learning. *Proc. IEEE* 109, 1 (2020), 43–76.